



## Research article

# Evaluating the effect of remote sensing image spatial resolution on soil exchangeable potassium prediction models in smallholder farm settings



Yiming Xu <sup>a, b, c, \*</sup>, Scot E. Smith <sup>a, b</sup>, Sabine Grunwald <sup>a, d</sup>, Amr Abd-Elrahman <sup>b, e</sup>,  
Suhas P. Wani <sup>f</sup>

<sup>a</sup> School of Natural Resource and Environment, University of Florida, 103 Black Hall, PO Box 116455, Gainesville, FL, 32611, USA

<sup>b</sup> School of Forest Resources and Conservation – Geomatics Program, University of Florida, 301 Reed Lab, PO Box 110565, Gainesville, FL, 32611-0565, USA

<sup>c</sup> Department of Environmental Science and Engineering, Beijing Technology and Business University, Beijing, 100048, China

<sup>d</sup> Pedometrics, Landscape Analysis and GIS Laboratory, Soil and Water Science Department, University of Florida, 2181 McCarty Hall, PO Box 110290, Gainesville, FL, 32611, USA

<sup>e</sup> Gulf Coast REC/School of Forest Resources and Conservation – Geomatics Program, University of Florida, 1200 N. Park Road, Plant City, FL, 33563, USA

<sup>f</sup> International Crops Research Institute for the Semi-Arid Tropics (ICRISAT), Patancheru, 502324, Hyderabad, India

## ARTICLE INFO

## Article history:

Received 21 December 2016

Received in revised form

7 June 2017

Accepted 8 June 2017

## Keywords:

Remote sensing

Digital soil mapping

Very fine resolution image

Soil exchangeable potassium

Smallholder farm settings

## ABSTRACT

Major end users of Digital Soil Mapping (DSM) such as policy makers and agricultural extension workers are faced with choosing the appropriate remote sensing data. The objective of this research is to analyze the spatial resolution effects of different remote sensing images on soil prediction models in two smallholder farms in Southern India called Kothapally (Telangana State), and Masuti (Karnataka State), and provide empirical guidelines to choose the appropriate remote sensing images in DSM. Bayesian kriging (BK) was utilized to characterize the spatial pattern of exchangeable potassium ( $K_{ex}$ ) in the topsoil (0–15 cm) at different spatial resolutions by incorporating spectral indices from Landsat 8 (30 m), RapidEye (5 m), and WorldView-2/GeoEye-1/Pleiades-1A images (2 m). Some spectral indices such as band reflectances, band ratios, Crust Index and Atmospherically Resistant Vegetation Index from multiple images showed relatively strong correlations with soil  $K_{ex}$  in two study areas. The research also suggested that fine spatial resolution WorldView-2/GeoEye-1/Pleiades-1A-based and RapidEye-based soil prediction models would not necessarily have higher prediction performance than coarse spatial resolution Landsat 8-based soil prediction models. The end users of DSM in smallholder farm settings need select the appropriate spectral indices and consider different factors such as the spatial resolution, band width, spectral resolution, temporal frequency, cost, and processing time of different remote sensing images. Overall, remote sensing-based Digital Soil Mapping has potential to be promoted to smallholder farm settings all over the world and help smallholder farmers implement sustainable and field-specific soil nutrient management scheme.

© 2017 Elsevier Ltd. All rights reserved.

## 1. Introduction

Soil fertility is an important limiting factor in arid and semi-arid agricultural ecosystem environments (Chander et al., 2014). The farmland ecosystems in smallholder farms display complex and

heterogeneous landscape features such as vegetation cover, land use, organisms, soil parent materials, and relief, which affect the distribution of the major soil properties. Remote sensing images with different spatial resolutions can provide landscape information at various scales in Digital Soil Mapping (DSM) research in smallholder farm settings. However, there is an ongoing debate and discussion about the appropriate remote sensing products to be used in DSM (Cavazzi et al., 2013; Vasques et al., 2012). Major end users of DSM such as policy makers and agricultural extension workers usually face the problem of choosing the appropriate remote sensing data (Pons-Fernández et al., 2004). The soil maps

\* Corresponding author. Department of Environmental Science and Engineering, Beijing Technology and Business University, Beijing, 100048, China.

E-mail addresses: [xuyimi@ufl.edu](mailto:xuyimi@ufl.edu) (Y. Xu), [sesmith@ufl.edu](mailto:sesmith@ufl.edu) (S.E. Smith), [sabgru@ufl.edu](mailto:sabgru@ufl.edu) (S. Grunwald), [aamr@ufl.edu](mailto:aamr@ufl.edu) (A. Abd-Elrahman), [s.wani@cgiar.org](mailto:s.wani@cgiar.org) (S.P. Wani).

with coarse spatial resolution were not appropriate for meaningful soil and land management, especially in fine scale areas such as smallholder farm settings. Coarser environmental variables may generalize landscape attributes, thus losing their predictive capability (Cavazzi et al., 2013). Soil maps with fine spatial resolutions may demand more processing time and higher costs of labor and image purchasing (Blasch et al., 2015). Quantifying the scale dependent relationships between soil properties and spectral indices from different remote sensing images can help end users choose the most appropriate remote sensing products in DSM, and provide site-specific soil management suggestions in smallholder farm settings.

Some research demonstrated that the incorporation of fine spatial resolution spectral indices can enhance the prediction accuracy of soil prediction models (Taylor et al., 2013). They demonstrated that soil depth modelling can attain the highest accuracy by utilizing terrain attributes with the finest spatial resolution. However, more and more research have concluded that the finer spatial resolution environmental variables may not always be the best choice in DSM. Kim et al. (2014) concluded that there was no significant distinction of model accuracy among soil TP and TN prediction models based on remote sensing images with different spatial resolutions in the Everglades in Florida. Maynard and Johnson (2014) showed that using high spatial resolution LiDAR data set with high cost and high computational requirements did little to improve the soil prediction model accuracy compared with the moderate resolution Digital Elevation Models (DEMs). With the development of commercial remote sensing sensors, various spectral indices with high spatial resolutions have been utilized in DSM in recent years (De Benedetto et al., 2013; Kim et al., 2014). Most of the previous research just compared the effects of remote sensing images with coarse and medium spatial resolutions such as MODIS and Landsat ETM+ on soil prediction models. Those research did not compare the model performance of Very High Resolution ( $\leq 5$  m) image-based soil prediction models and medium spatial resolution (30 m) image-based soil prediction models. The utilization of Very High Resolution (VHR) images such as Pleiades-1A and RapidEye in DSM in smallholder farm is still in its infancy.

This research 1) analyzed the relationships between soil exchangeable potassium ( $K_{ex}$ ) and spectral indices extracted from WorldView-2/GeoEye-1/Pleiades-1A (2 m), RapidEye (5 m), and Landsat 8 imagery (30 m) in two smallholder farms called Kothapally and Masuti; 2) characterized the spatial pattern of soil  $K_{ex}$  in the two study areas by soil prediction models based on those remote sensing images; 3) assessed the effects of different remote sensing images on soil prediction models; and 4) discussed the empirical guidelines to select the appropriate spectral indices and remote sensing images in DSM.

## 2. Materials and methods

### 2.1. Description of two study areas

Kothapally is a smallholder village located in Ranga Reddy District, Telegana State, India. It is located between  $17^{\circ} 20'$  to  $17^{\circ} 24'N$  latitude and  $78^{\circ} 5'$  to  $78^{\circ} 8'E$  longitude, with an area of about  $10 \text{ km}^2$ , an elevation of 600–640 m, and an average slope of 2.5%. It experiences a hot and dry semi-arid climate with the annual rain fall of 802 mm (1999–2008). The monsoon season is from June to September with the precipitation about 755 mm. In general, 90% of the areas in Kothapally are Vertisols. More than 95 percent area of the Kothapally was planted with cotton (*Gossypium hirsutum*) during the rainy season. Sorghum (*Sorghum bicolor*), tomato (*Lycopersicon esculentum* var. *esculentum*), onion (*Allium cepa*) and

maize (*Zea mays*) were major crops in dry season (Wani et al., 2003).

Masuti (latitude  $16^{\circ} 28'$  to  $16^{\circ} 33'N$  and longitude  $75^{\circ} 45'$  to  $75^{\circ} 50'E$ , elevation 520–630 m) is one of 125 villages situated in Basavana bagevadi tehsil, Bijapur district of Karnataka State, India. The district experiences a semi-arid climate with temperature variations between  $20^{\circ}C$  and  $42^{\circ}C$ . The rainfall varies from 569 to 595 mm. The soils in this area are dark greyish brown and dark brown to dark reddish brown in color. Soil texture varies from loam to clay. The infiltration characteristics of these soils are moderate to good. Cotton (*Gossypium hirsutum*), rice (*Oryza sativa*), and maize (*Zea mays*) are the three major crops in the rainy season. Sorghum (*Sorghum bicolor*), tomato (*Lycopersicon esculentum* var. *esculentum*), and onion (*Allium cepa*) are the three major crops in the dry season. Irrigation facilities such as dams and canals are located in the southwest section of the village, and about 80% of the village is irrigated using wells (Sreedevi et al., 2004).

### 2.2. Soil sampling and laboratory analysis

A total of 255 soil samples at 0–15 cm were collected in Kothapally in May 2012 (Xu et al., 2017), and a total of 259 soil samples at 0–15 cm were collected in Masuti in February to March 2013 by International Crops Research Institute for the Semi-Arid Tropics (ICRISAT) and University of Florida Team (Fig. 1). Site-specific descriptions, including land use, crop, and topography, as well as x and y coordinates, were recorded at each sampling point. Each soil sampling location was measured by Trimble GEOXT2005 (Trimble Navigation Ltd., Sunnyvale, California, USA). Global Positioning System (GPS) post-correction was performed by Aimil Ltd. ([www.aimil.com](http://www.aimil.com)) in Hyderabad, India. All the soil samples were air-dried for one week, and they were then sieved using a 2-mm sieve for laboratory analysis in the soil laboratory at ICRISAT. Each soil sample in two study areas was analyzed for exchangeable potassium ( $K_{ex}$ ) (Thomas, 1982).

### 2.3. Environmental variables

#### 2.3.1. Remote sensing data collection

In Kothapally, two Landsat 8 images (30 m), two RapidEye images (5 m) and a single WorldView-2 and a single GeoEye-1 image (2 m) were collected (Table S1). In Masuti, two Landsat 8 images, two RapidEye images and a single WorldView-2 and a single Pleiades-1A image (2 m) were also acquired (Table S1). All the remote sensing images were obtained in dry season. Advanced Spaceborne Thermal Emission and Reflection Radiometer (ASTER) Global Digital Elevation Model (DEM) of the two study areas were obtained from United States Geological Survey (USGS) website.

#### 2.3.2. Remote sensing data processing

After applying radiometric calibration to all images, the digital numbers of the remote sensing products were transformed to at-sensor radiance. The radiance images were converted to surface reflectance using the Fast Line-of-Site Atmospheric Analysis of Spectral Hypercubes (FLAASH) atmospheric correction tool in the ENVI 5.0 software. Geometric correction was applied to all the images with 10 control points collected by a Global Navigation Satellite System (GNSS) post-processed to sub-meter accuracy. The “Georeferencing” toolbar in ArcGIS 10 was used to perform the geometric correction with nearest neighborhood resampling. The Root Mean Square Error (RMSE) was smaller than 0.5 pixel for each control point.

#### 2.3.3. Environmental variable extraction

The band reflectances, the band ratios, and multiple spectral

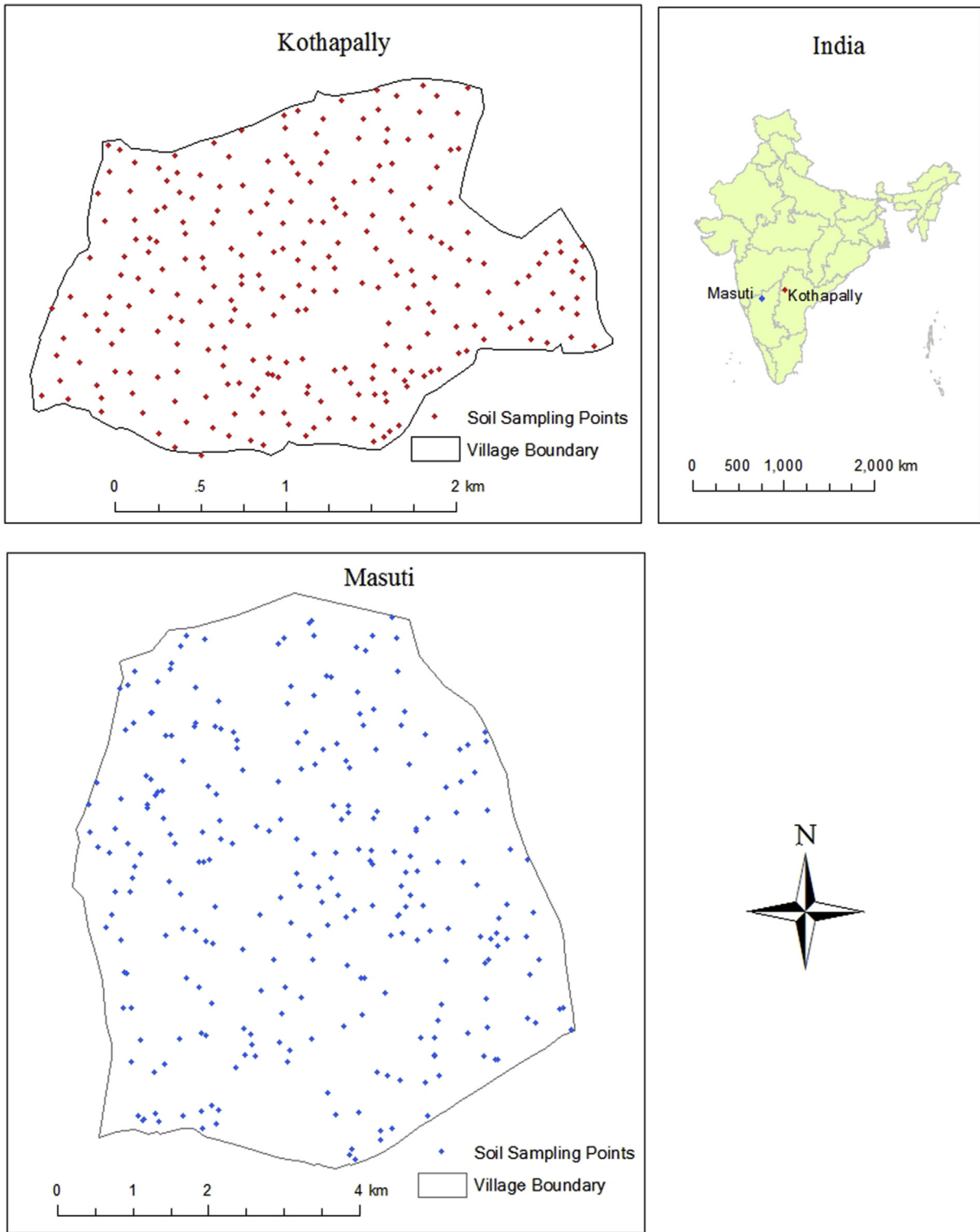


Fig. 1. The soil sampling sites in Kothapally and Masuti Village, India.

indices were extracted from each remote sensing image. Topographic attributes such as elevation, aspect, flow accumulation were extracted from DEM. In addition, geographic attributes such as x and y coordinates of each soil sample point were also collected. The detailed description of the environmental variables acquired in this research were listed in Table S2.

#### 2.4. Bayesian geostatistical model

This research utilized a trans-normal spatial linear mixed model (Eq. (1)) (Diggle et al., 1998; Xiong et al., 2015) to build soil  $K_{ex}$  prediction models:

$$Y(u) = X(u)\beta + S(u) + \varepsilon(u) \quad (1)$$

where  $Y(u)$  is the target random variable (e.g., soil  $K_{ex}$ ) at location  $u$ ;  $X$  presents a design matrix of fixed effects including the intercept at location  $u$ , and  $\beta$  is a vector of model parameter;  $S(u)$  represents the spatial random effects with multivariate normal distribution,  $S(u) \sim N(0, \sigma^2 R(h; \varphi))$ , where  $R(h; \varphi)$  is a correlation matrix,  $h$  is the distance of two locations,  $\varphi$  is the range parameter and  $\sigma^2$  is partial sill; and  $\varepsilon(u)$  is a vector of the errors with  $\varepsilon(u) \sim N(0, \tau^2 I)$  where  $I$  is an  $n$ -dimensional identity matrix, and  $\tau^2$  is nugget variance. The estimation of correlation parameters and fixed effects coefficients in Eq. (1) were obtained by restricted maximum likelihood estimation (REML) (Cressie, 1993; Finley et al., 2007).

In this study, the covariance (element of the covariance matrix  $\sigma^2 R(h; \varphi)$ ) was modelled by the exponential correlation function (Eq. (2)) or spherical correlation function (Eq. (3)):

$$R(h; \varphi) = \exp\left(-\frac{h}{\varphi}\right) \quad (2)$$

$$R(h; \varphi) = \begin{cases} c_0 \left[ \frac{3}{2} \frac{h}{\varphi} - \frac{1}{2} \left(\frac{h}{\varphi}\right)^3 \right], & \text{for } h \leq \varphi \\ c_0 & \text{for } h > \varphi \end{cases} \quad (3)$$

Markov Chain Monte Carlo (MCMC) simulation proceeds via Gibbs sampler in the R software “spBayes” package (Finley et al., 2007) were applied for the Bayesian computation in this study. Prior parameter distribution, starting and tuning parameters were specified according to the previous variogram analysis. Three MCMC chains were run for 15,000 iterations for each model. Out of the 15,000 iterations, the 5000 iterations before the convergence were discarded and the remaining 10,000 iterations were retained to derive posterior distributions of the model parameters and predictions. Several R packages such as “spBayes”, “geoR”, “lattice”, “mapproj”, and “rgdal” were utilized to build the soil prediction models and map soil  $K_{ex}$ .

### 2.5. Model validation

For all the soil prediction models in Kothapally, soil sample points were split 70/30 into a calibration set (179) for model calibration, and a validation set (76) for independent model validation. For all the soil prediction models in Masuti, soil sample points were also split 70/30 into a calibration set (180) for model calibration, and a validation set (79) for independent model validation. The Kolmogorov-Smirnov test was applied for the soil  $K_{ex}$  calibration and validation datasets to ensure they have the same distribution.

Log-transform was applied to the whole dataset, calibration dataset, and validation dataset to approach the normal distribution of soil  $K_{ex}$ . The coefficient of determination ( $R^2$ ), root mean squared error (RMSE), residual prediction deviation (RPD) (Bellon-Maurel et al., 2010), and ratio of performance to inter-quartile distance (RPIQ) (Williams and Norris, 1987) were used to compare different Bayesian kriging models.

## 3. Results

### 3.1. Characteristics of soil exchangeable potassium in two study areas

Table 1 showed soil  $K_{ex}$  distribution and log-transformed soil  $K_{ex}$  distribution at 0–15 cm in two study areas. Soil  $K_{ex}$  had a mean of 241.64 mg kg<sup>-1</sup>, a median of 231.06 mg kg<sup>-1</sup>, and a range of 55.90–615 mg kg<sup>-1</sup> in Kothapally. Soil  $K_{ex}$  had a mean of 129.71 mg kg<sup>-1</sup>, a median of 107.11 mg kg<sup>-1</sup>, and a range of 28–962 mg kg<sup>-1</sup> in Masuti. Soil  $K_{ex}$  showed positive skewed distribution in both study areas. After the log-transformation, soil  $K_{ex}$  approached Gaussian distribution in both study areas. The similarity between the calibration, validation, and whole datasets suggested that the calibration and validation datasets of soil  $K_{ex}$  were representative.

### 3.2. Linear relationship between soil $K_{ex}$ and spectral indices with different spatial resolutions

#### 3.2.1. Correlations between soil $K_{ex}$ and spectral indices in Kothapally

Table 2 shows the Spearman's rank correlation coefficients between the soil  $K_{ex}$  and the spectral indices from different remote sensing images in Kothapally. The band ratios between the visible bands such as green to blue (GB) and red to blue (RB), and the band reflectances from all the remote sensing images had relatively strong negative correlations with  $K_{ex}$ . For the spectral indices from Landsat 8, only Crust Index (CI) from Landsat 8 showed positive correlations with  $K_{ex}$ . For the spectral indices from RapidEye, only CI and Atmospherically Resistant Vegetation Index (ARVI) showed positive correlations with  $K_{ex}$ . The near infrared indices, such as ARVI, Normalized Difference Vegetation Index (NDVI), and Transformed Vegetation Index (TVI), and the red edge-related indices, such as Normalized Difference Red-edge Index (NDVIr), the band ratio of NIR band 1 to red edge band (N1RE) from WorldView-2, had relatively strong positive correlations with  $K_{ex}$ .

#### 3.2.2. Correlations between soil $K_{ex}$ and spectral indices in Masuti

Table 3 shows the Spearman's rank correlation coefficients

**Table 1**  
Description of raw and log-transformed soil  $K_{ex}$  at 0–15 cm in two study areas.

Location	Transform	Data Type	N	Mean (mg/kg)	Median (mg/kg)	SD	Min (mg/kg)	Max (mg/kg)	Range (mg/kg)	Skew	Kurtosis	CV
Kothapally		Total	255	242	231	110	55	615	560	0.65	0.13	0.46
		Calibration	179	242	229	108	55	615	560	0.64	0.07	0.45
		Validation	76	241	232	116	60	607	547	0.66	0.11	0.48
	log <sub>10</sub> (x)	Total	255	2.34	2.36	0.21	1.74	2.79	1.05	-0.43	-0.27	0.09
		Calibration	179	2.34	2.36	0.21	1.74	2.79	1.05	-0.4	-0.3	0.09
		Validation	76	2.33	2.37	0.23	1.78	2.78	1.01	-0.46	-0.38	0.10
Masuti		Total	259	130	107	101	28	962	933	3.91	24.36	0.78
		Calibration	180	129	108	94	28	741	713	3.06	15.18	0.73
		Validation	79	132	99	116	39	962	923	4.73	30.51	0.88
	log <sub>10</sub> (x)	Total	259	2.03	2.03	0.26	1.45	2.98	1.53	0.32	0.13	0.13
		Calibration	180	2.03	2.03	0.26	1.45	2.87	1.42	0.22	-0.12	0.13
		Validation	79	2.03	2.00	0.26	1.59	2.98	1.40	0.55	0.62	0.13

Abbreviations: N, number of samples; SD, standard deviation; CV, coefficient of variation.

**Table 2**

Linear correlations between soil  $K_{ex}$  and spectral indices at 255 soil sampling sites (0–15 cm) in Kothapally.

Landsat 8		RapidEye		WVa and GE	
Index	R	Index	R	Index	R
LtBGB	-0.537	REaRededge	-0.468	WVaARVI	0.489
LtAGB	-0.511	REbRededge	-0.453	WVaYellow	-0.477
LtBGreen	-0.510	REbGreen	-0.432	WVaRed	-0.471
LtBci	0.493	REbREB	-0.425	WVaCI	0.467
LtBRB	-0.493	REaNIR	-0.384	WVaRB	-0.467
LtBRed	-0.487	REbGB	-0.378	WVaGreen	-0.464
LtBSWIR1	-0.469	REaGreen	-0.375	WVaBlue	-0.440
LtBBlue	-0.453	REbNIR	-0.375	WVaN2R	0.429
LtAGreen	-0.450	REaRed	-0.374	WVaRG	-0.423
LtBS1B	-0.441	REaREB	-0.368	WVaNDVIR	0.421
LtACI	0.431	REbRed	-0.355	WVaCIr	0.421
LtARB	-0.431	REbBlue	-0.352	WVaN1RE	0.421
LtBRG	-0.429	REaBlue	-0.345	WVaN2RE	0.421
LtARed	-0.418	REbCI	0.318	GEGreen	-0.420
LtBCoastal	-0.402	REbRB	-0.318	WVaNDVI	0.418
LtBSWIR2	-0.396	REbARVI	0.296	WVaSR	0.418
LtASWIR1	-0.393	REaREG	-0.294	WVaTVI	0.418

Nomenclature of the variable in Table 2: Remote sensing image (Abbreviation in Table S1) + Spectral index (Abbreviation in Table S2).

Abbreviations: R, Spearman's rank correlation coefficient; WVa, WorldView-2 image (2011-12-14); GE, GeoEye image (2011-1-21).

between soil  $K_{ex}$  and spectral indices with different spatial resolutions in Masuti. The correlation coefficients between  $K_{ex}$  and the spectral indices in Masuti were generally higher than those in Kothapally. For the spectral indices from the Landsat 8 images, bare soil index (LTabSI) incorporating Short Wavelength Infrared (SWIR), Near Infrared (NIR), and visible bands had the strongest correlation with  $K_{ex}$  ( $R: -0.697$ ). Other SWIR-related spectral indices such as Moisture Stress Index (MSI), and Normalized Difference Soil Index (NDSI) all showed relatively strong negative linear relationships with  $K_{ex}$ . Linear correlations between SWIR-related spectral indices and  $K_{ex}$  were generally stronger compared with those between NIR-related vegetation indices and  $K_{ex}$  in Masuti.

The band reflectances and the band ratios between visible bands from WorldView-2, Pleiades-1A, and RapidEye demonstrated

**Table 3**

Linear correlations between soil  $K_{ex}$  and spectral indices at 259 soil sampling sites (0–15 cm) in Masuti.

Landsat 8		RapidEye		WVb and PL	
Index	R	Index	R	Index	R
LtCBSI	-0.697	REdRededge	-0.606	PLRG	-0.604
LtDBSI	-0.676	REdCI	0.588	PLARVI	0.604
LtCARVI	0.668	REdRB	-0.588	PLCI	0.604
LtDCI	0.661	REdRed	-0.588	PLRB	-0.604
LtDRB	-0.661	REcRededge	-0.584	WVbARVI	0.58
LtCNDWI	0.645	Ycoor	-0.578	Ycoor	-0.578
LtCMSI	-0.645	REcCI	0.572	PLRed	-0.57
LtCNDSI	-0.645	REcRB	-0.572	WVbYellow	-0.563
LtCS1N	-0.645	REdGreen	-0.566	WVbCI	0.56
LtDNDWI	0.633	REcRed	-0.563	WVbRB	-0.56
LtDMSI	-0.633	REcGreen	-0.542	WVbRed	-0.546
LtDNDSI	-0.633	REcARVI	0.531	PLGB	0.545
LtDS1N	-0.633	REdARVI	0.514	WVbGreen	-0.526
LtDRG	-0.631	Elevation	-0.51	PLBlue	-0.522
LtDRed	-0.63	REdRG	-0.504	WVbNDVI	0.516
LtDARVI	0.626	REdBlue	-0.501	WVbSR	0.516
LtDSWIR1	-0.621	REcBlue	-0.491	WVbTVI	0.516

Nomenclature of the variable in Table 3: Remote sensing image (Abbreviation in Table S1) + Spectral index (Abbreviation in Table S2).

Abbreviations: R, Spearman's rank correlation coefficient; WVb, WorldView-2 image (2011-2-28); PL, Pleiades-1A image (2013-3-3).

relatively strong negative correlations with  $K_{ex}$ . Crust Index (CI) and ARVI from WorldView-2, Pleiades-1A, and RapidEye, and NIR-related indices such as NDVI, ARVI, and TVI, and red edge-related indices such as NDVIR and CIr from WorldView-2 showed relatively strong positive correlations with  $K_{ex}$ .

### 3.3. Multi-linear trend models between soil $K_{ex}$ and the spectral indices

Multi-linear regression models K1, K2 and K3 were built to relate log-transformed soil  $K_{ex}$  and spectral indices from Landsat 8, RapidEye, WorldView-2/GeoEye-1 respectively in Kothapally (Table 4). Multi-linear regression models M1, M2 and M3 were also built to relate log-transformed soil  $K_{ex}$  and spectral indices from Landsat 8, RapidEye, WorldView-2/Pleiades-1A respectively in Masuti (Table 4). Those spectral indices in the models K1, K2, and K3 were selected as covariates in Bayesian Kriging (BK) models KB1, KB2, and KB3 in Table 5. Those spectral indices in the models M1, M2, and M3 were also selected as covariates in BK models MB1, MB2, and MB3 in Table 5.

### 3.4. Bayesian geostatistical models of soil $K_{ex}$

#### 3.4.1. Spatial pattern of soil $K_{ex}$ at different spatial resolutions in Kothapally

$K_{ex}$  posterior mean prediction maps from models KB1 to KB3 are shown in Fig. 2. In the southwestern, northwestern, and eastern areas of the Kothapally village,  $K_{ex}$  is relatively lower compared with other areas. The southwestern area of the Kothapally village is monoculture where only cotton is planted in rainy season.  $K_{ex}$  was relatively high in the central and southeastern areas of the village, where crop rotation agricultural system is the major system. The line pattern (lower  $K_{ex}$  area) mosaicked in the patch pattern (higher  $K_{ex}$  area) demonstrated the low  $K_{ex}$  of the road across the high  $K_{ex}$  of the farmland as shown by model KB3 (Fig. 2 (C)). On the contrary, the relative homogeneous spatial pattern of  $K_{ex}$  from model KB1 “simplified” the  $K_{ex}$  distribution in small agricultural fields in Kothapally.

The soil  $K_{ex}$  patterns in Farmland A in Kothapally from the three models generally resembled each other, and the three models all show that the northern and southeastern areas of the Farmland A had relatively low  $K_{ex}$  (Fig. 3). The high  $K_{ex}$  variations in field blocks, and different linear and polygon patterns of  $K_{ex}$  were clearly characterized by soil  $K_{ex}$  map based on WorldView-2 and GeoEye-1 (Fig. 3 (C)). On the contrary, there was no evident linear and patch  $K_{ex}$  pattern shown in soil  $K_{ex}$  map based on Landsat 8 (Fig. 3 (A)). Bayesian kriging method provides a confident interval for soil  $K_{ex}$  prediction. Fig. S1 showed 2.5 and 97.5 percentile of  $K_{ex}$  prediction from Model KB1, KB2 and KB3. Generally, the 2.5 percentile prediction maps from the three BK models showed a similar spatial pattern. The 97.5 percentile prediction map from model KB3 (Fig. S1 (F)) displayed larger areas with  $K_{ex}$  larger than  $600 \text{ mg kg}^{-1}$ . There is a 95% probability that the soil  $K_{ex}$  concentration value at a pixel was between the 2.5 and 97.5 percentile of  $K_{ex}$  prediction maps.

Table 5 indicated that BK model based on Landsat 8 (KB1) attained the highest prediction fit ( $R^2 = 0.57$ ) and lowest prediction error ( $\text{RMSE} = 77.35 \text{ mg kg}^{-1}$ ) compared with the BK models based on WorldView-2 and GeoEye-1 ( $R^2 = 0.52$ ;  $\text{RMSE} = 80.55 \text{ mg kg}^{-1}$ ) and RapidEye ( $R^2 = 0.47$ ;  $\text{RMSE} = 83.91 \text{ mg kg}^{-1}$ ). Those results suggested that the spectral indices with fine spatial resolution did not bring in a higher model performance for the soil  $K_{ex}$  prediction model in Kothapally.

#### 3.4.2. Spatial pattern of $K_{ex}$ at different spatial resolutions in Masuti

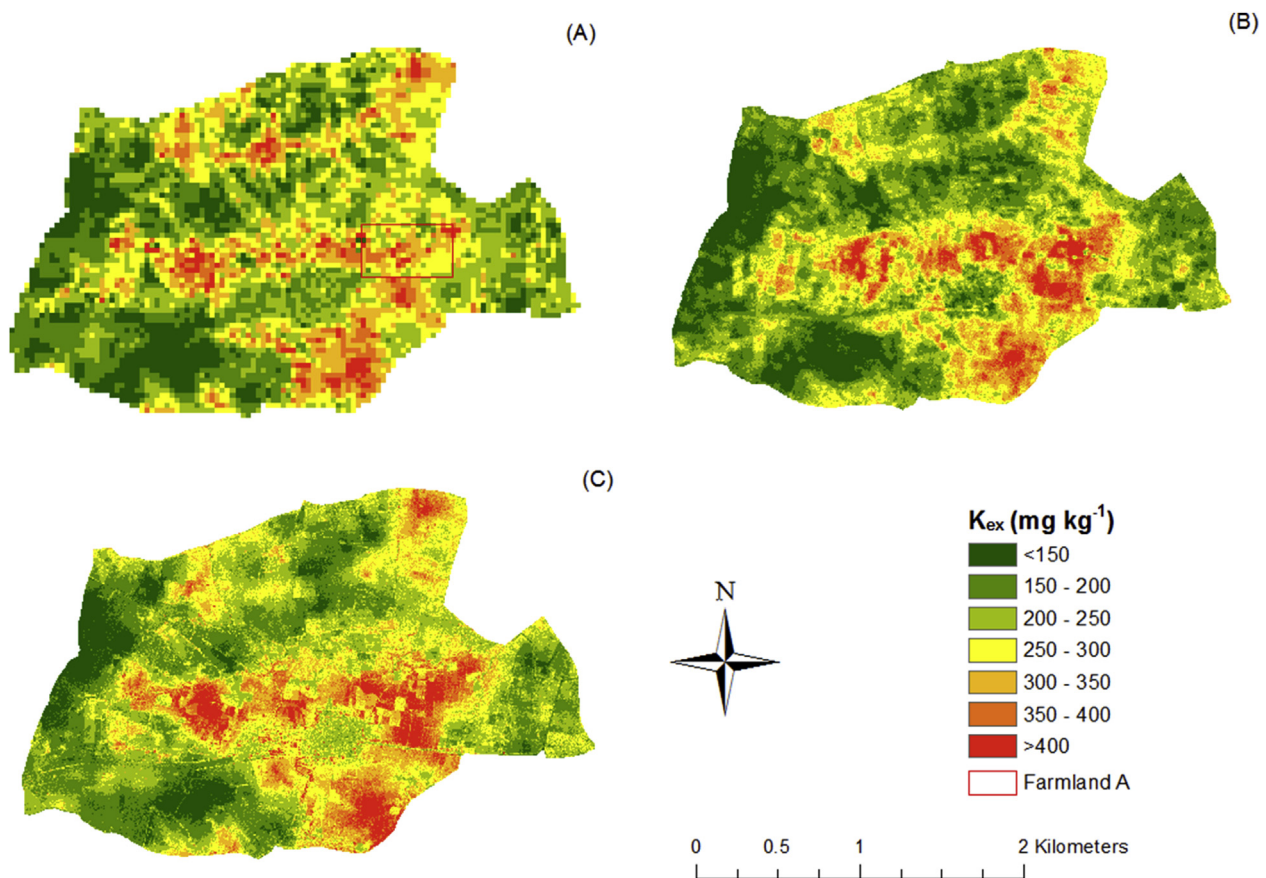
The spatial pattern of soil  $K_{ex}$  based on models MB1, MB2 and

**Table 4**  
Multi-linear trend models of soil  $K_{ex}$  in two study areas.

Model	Multi-linear trend model	Spatial resolution (m)	R <sup>2</sup>	Location
K1	$\log K_{ex} = 1.83 + 0.11 * LTaGB - 0.11 * LTbCI - 5.53 * LTbBSI - 0.68 * LTbNB + 1.29 * LTbS2G$	30	0.34	Kothapally
K2	$\log K_{ex} = 3.01 - 3.83 * REbRededge - 0.24 * REbARVI + 0.08 * REbCI - 0.025 * Slope$	5	0.27	Kothapally
K3	$\log K_{ex} = 2.37 - 0.13 * WVaN2R + 0.11 * WVaN2G - 0.1 * WVaREB + 0.91 * WVaARVI$	2	0.29	Kothapally
M1	$\log K_{ex} = 2.09 - 6.13 * LTdBSI - 4.12 * LTdNDWI + 0.40 * LTcARVI$	30	0.33	Masuti
M2	$\log K_{ex} = 1.89 - 1.83 * REcRededge + 0.05 * REcARVI + 0.57 * REcCI$	5	0.28	Masuti
M3	$\log K_{ex} = 1.57 - 4.80 * WVbBlue + 1.28 * WVbN2RE - 0.28 * WVbN1B + 0.49 * PLARVI$	2	0.40	Masuti

**Table 5**  
Validation results of Bayesian Kriging for  $K_{ex}$  in two study areas.

Model	Covariates	Adj R <sup>2</sup>	RMSE (mg kg <sup>-1</sup> )	RPD	RPIQ	Spatial resolution (m)	Location
KB1	LTaGB, LTbCI, LTbBSI, LTbNB, LTbS2G	0.57	77.35	1.50	1.89	30	Kothapally
KB2	REaARVI, REbRed, REbCI	0.47	83.91	1.38	1.74	5	Kothapally
KB3	GECl, Slope, WVaBlue, WVaNDVIr	0.52	80.55	1.43	1.82	2	Kothapally
MB1	LTbBSI, LTbNDWI, LTaARVI	0.54	49.14	1.47	1.98	30	Masuti
MB2	REaRededge, REaARVI, REaCI	0.42	54.80	1.32	1.78	5	Masuti
MB3	WVbBlue, WVbN2RE, WVbN1B, PLARVI	0.55	48.11	1.50	2.03	2	Masuti

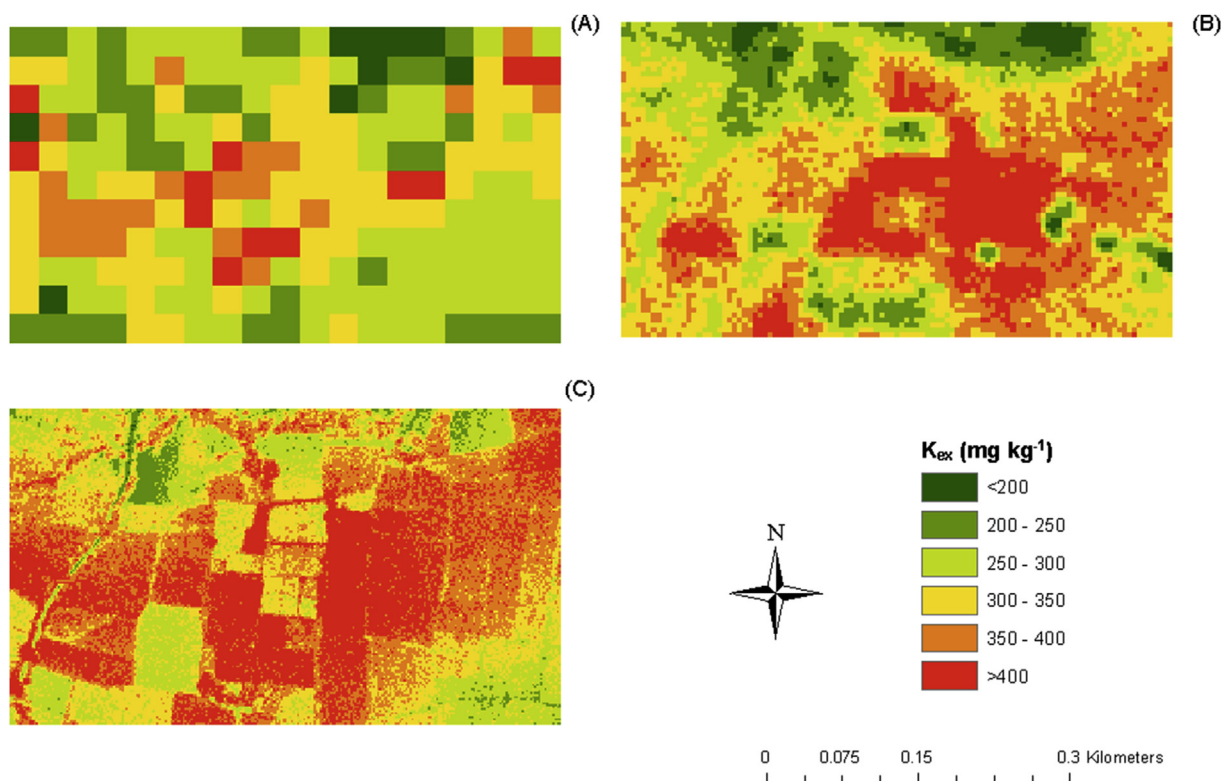


(A): The spectral indices were extracted from Landsat 8 images (Acquisition date: 2013-4-13; 2013-4-29).  
(B): The spectral indices were extracted from RapidEye images (Acquisition date: 2010-4-19; 2013-2-24).  
(C): The spectral indices were extracted from WorldView-2 (Acquisition date: 2011-12-14) and GeoEye-1 images (Acquisition date: 2012-1-21).

**Fig. 2.** Posterior soil exchangeable potassium ( $K_{ex}$ ) prediction at 0–15 cm depth in Kothapally from (A) Model KB1; (B) Model KB2; (C) Model KB3.

MB3 is shown in Fig. 4. Three maps in Fig. 4 showed a similar  $K_{ex}$  spatial pattern. Soil  $K_{ex}$  is relatively higher in the southwestern area of the village compared with other areas (Fig. 4). In this area, a crop-rotation system was used where sugarcane is the main crop type in

the dry season. The irrigation canal in the southwestern area of the village also may bring more water and increase soil moisture in the region.  $K_{ex}$  is relatively lower in the northern area of the village where most areas are permanent fallow land and the main soil type



(A): The spectral indices were extracted from Landsat 8 images (Acquisition date: 2013-4-13; 2013-4-29).  
 (B): The spectral indices were extracted from RapidEye images (Acquisition date: 2010-4-19; 2013-2-24).  
 (C): The spectral indices were extracted from WorldView-2 (Acquisition date: 2011-12-14) and GeoEye-1 images (Acquisition date: 2012-1-21).

**Fig. 3.** Posterior soil  $K_{ex}$  prediction at 0–15 cm depth in Farmland A in Kothapally from (A) Model KB1; (B) Model KB2; (C) Model KB3.

is Entisols. The farmland in the north central area of the village close to a dam also had relatively high  $K_{ex}$ . Vertisols is the main soil type in the southern area of village. This soil type is rich in montmorillonite clay and has a relatively high exchangeable buffering capacity. Moisture-holding capacity of Vertisols is also relatively higher than Entisols in the northern area of the village. As a result, the  $K_{ex}$  in the southern area of the village is relatively higher than that in the northern area of the village. The heterogeneous spatial pattern of  $K_{ex}$  in Fig. 4 (C) demonstrated it can depict the complexity and variability of  $K_{ex}$ . Large areas in northern part of Masuti has  $K_{ex}$  smaller than  $150 \text{ mg kg}^{-1}$ , which is defined as low level by Horneck et al. (2011). It is possible that soil  $K_{ex}$  deficiency occur in the northern area of Masuti village.

Three maps in Fig. 5 showed the relatively low  $K_{ex}$  pattern in western area of Farmland B in Masuti, and relatively high  $K_{ex}$  pattern in the southeastern area of Farmland B in Masuti. In Fig. 5 (C), the widespread fragmented pattern of  $K_{ex}$  displayed the highly spatial variation of  $K_{ex}$  across the Farmland B, the point distribution of  $K_{ex}$  showed the subtle gradients of  $K_{ex}$  in single field block, and the evident line pattern of low  $K_{ex}$  (road) embedded in the patchy pattern of high  $K_{ex}$  (field blocks). The distinct planar distribution of  $K_{ex}$  demonstrated the different  $K_{ex}$  status in adjacent field blocks. In contrast, no specific spatial patterns of  $K_{ex}$  is evident in Fig. 5 (A).

Fig. S2 showed the 2.5 and 97.5 percentile of  $K_{ex}$  prediction from the three BK models. It suggests the specific pixel had a 95% probability to contain soil  $K_{ex}$  between the 2.5 and 97.5 percentile of  $K_{ex}$  prediction maps. Some areas had  $K_{ex}$  larger than  $150 \text{ mg kg}^{-1}$  in the 2.5 and 97.5 percentile of the  $K_{ex}$  prediction maps, suggesting

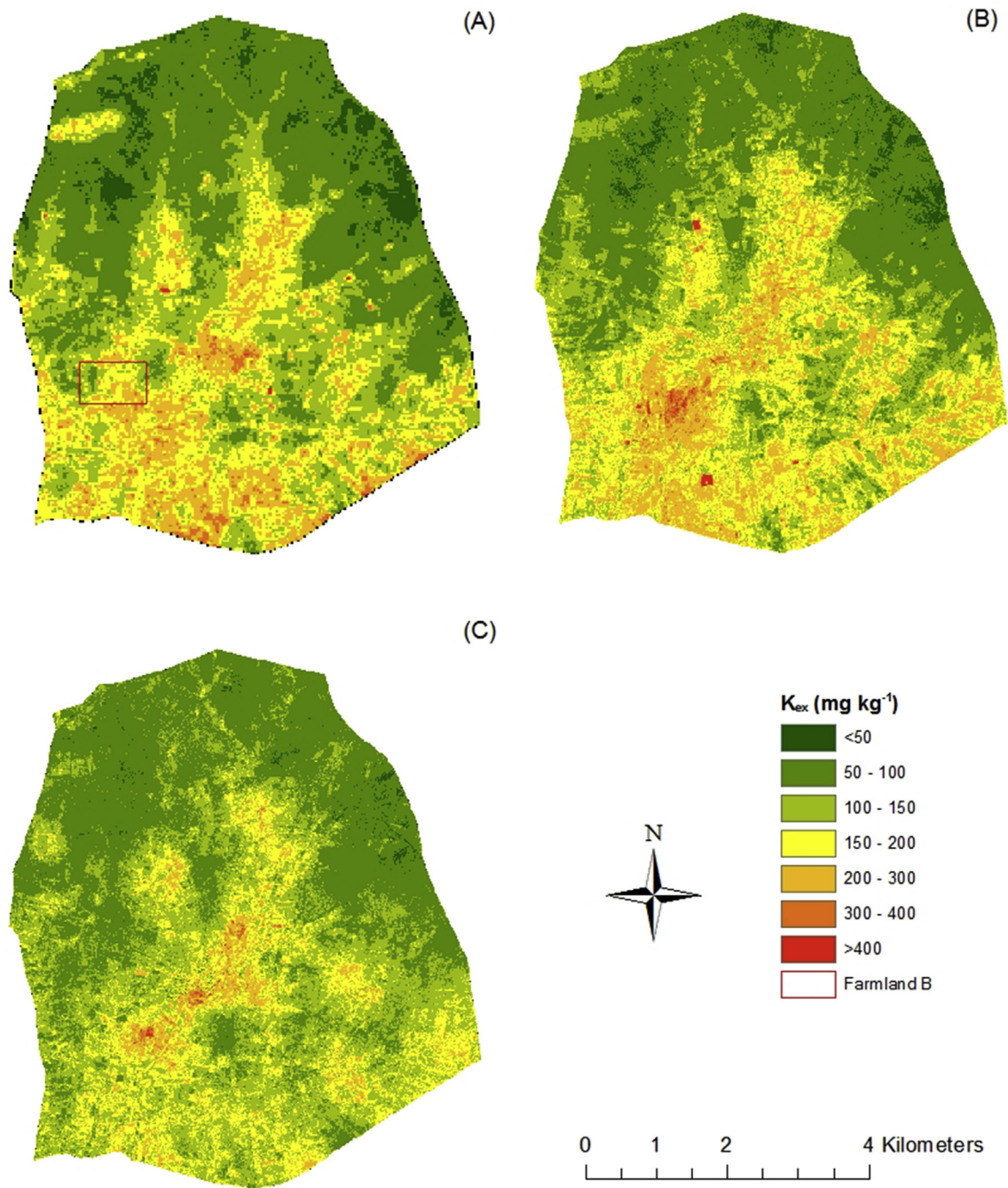
these areas had a 95% probability to contain  $K_{ex}$  larger than  $150 \text{ mg kg}^{-1}$ .

Similar to soil  $K_{ex}$  model in Kothapally, RapidEye-based soil  $K_{ex}$  model also attained the lowest prediction fit and highest prediction error among all the models in Masuti (Table 5). The Landsat-based (MB1) and WorldView-2/Pleiades-1A-based (MB3) soil  $K_{ex}$  prediction models did not demonstrate significant difference in terms of  $R^2$ , RMSE, RPD and RPIQ in Masuti.

## 4. Discussion

### 4.1. Characteristics of spectral indices from different remote sensing images

The Crust Index, ARVI, NDVI and SAVI; band ratios of NIR band to visible bands; and band ratios of red edge band to visible bands from all remote sensing images had relatively strong positive relationships with soil  $K_{ex}$ . The positive correlation between the vegetation indices (e.g. ARVI and NDVI) and soil  $K_{ex}$  indicates the importance of vegetation in retaining soil nutrients such as soil  $K_{ex}$  in smallholder farm settings. As a large absorption of leaf water occurs in the  $0.4\text{--}2.5 \mu\text{m}$  spectrum, the VIS-NIR and SWIR reflectance are negatively correlated to leaf water content (Liu et al., 2015). The relatively strong positive correlation between Crust Index and soil  $K_{ex}$  suggested that soil crusts can contribute to the conservation of soil  $K_{ex}$  in two study areas. The research from Rosentreter et al. (2014) and Belnap and Lange (2013) also indicated that soil crust in the arid and semiarid areas can improve water penetration, help soil microbial growth and soil



(A): The spectral indices were extracted from Landsat 8 (2013-04-20; 2013-05-22).

(B): The spectral indices were extracted from RapidEye (2012-12-11; 2013-1-5).

(C): The spectral indices were extracted from WorldView-2 (2011-2-28) and Pleiades-1A (2013-3-3).

**Fig. 4.** Posterior mean of soil  $K_{ex}$  prediction at 0–15 cm depth in Masuti from (A) Model MB1; (B) Model MB2; (C) Model MB3.

formation, and retain soil moisture. The negative correlations between band reflectance values and soil  $K_{ex}$  may suggest the land with more water contents (low band reflectance values) were prone to have more soil  $K_{ex}$ . As some SWIR band-related spectral indices such as BSI and NDSI can indicate the bare soil, the relatively strong negative linear correlations between them and soil  $K_{ex}$  suggested that bare soil were prone to contain less soil  $K_{ex}$  compared with vegetated areas in the two study areas. As a

traditional vegetation index, NDVI did not demonstrate strong correlations with soil  $K_{ex}$  in this research. In contrast, red edge-based spectral indices such as NDVIr from different remote sensing images demonstrated their high correlations with soil  $K_{ex}$ . It suggests that red edge-based spectral indices can help predict soil  $K_{ex}$  status. In areas where vegetation coverage is low and bare soil coverage is high, the brightness of soil and bare land may also influence the NDVI value (Qi et al., 1994). Another problem of

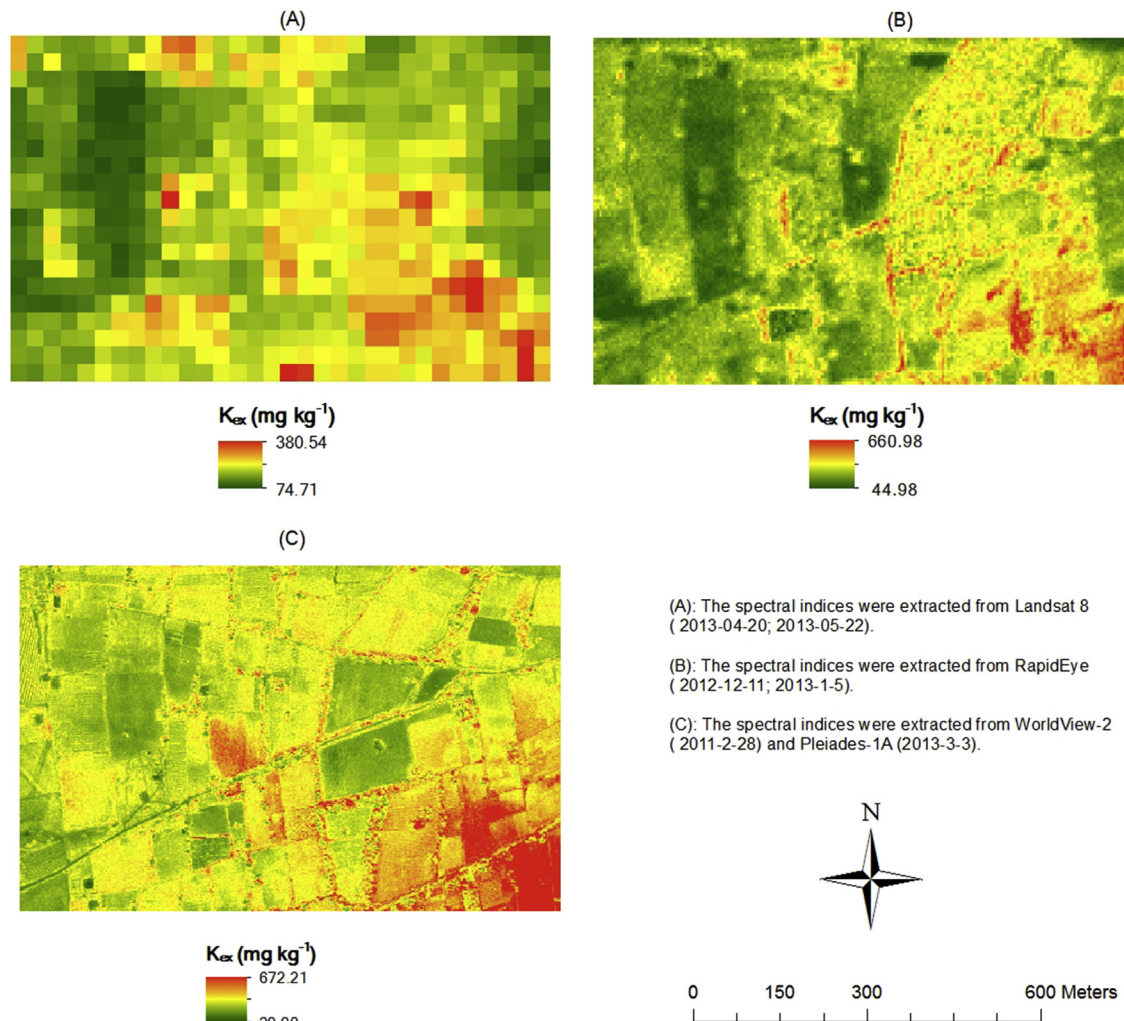


Fig. 5. Posterior mean of soil  $K_{ex}$  prediction at 0–15 cm depth in Farmland B in Masuti from (A) Model MB1; (B) Model MB2; (C) Model MB3.

using vegetation indices, particularly NDVI and Simple Ratio (SR) based on the red and NIR bands, is that they asymptotically approach a saturation level after a certain biomass density (Santin-Janin et al., 2009; Thenkabail et al., 2000). As a result, NDVI usually yields poor estimates of biomass in full canopy cover. In general, spectral indices including vegetation indices that correct the soil brightness and atmospheric effects, narrow band spectral indices such as red edge-related spectral indices that estimate biomass at full canopy cover, SWIR and thermal infrared (TIR)-related spectral indices that reflect soil moisture and temperature, and some bare soil indices that can characterize the bare soil and soil moisture would be preferable to be incorporated into soil prediction models in semi-arid areas.

The results indicated the behaviors of the spectral indices from different remote sensing images were similar in both study areas. Those environmental variables which have strong correlations with soil  $K_{ex}$  suggested the main factors that affect the spatial distribution of soil  $K_{ex}$  in two study areas. The relatively strong negative correlations ( $-0.51$ ) between elevation and  $K_{ex}$  in Masuti suggested relatively low elevation areas were prone to contain more  $K_{ex}$  than relatively high elevation areas. Due to the relatively small area of the smallholder farm, climate is not a major factor that affect the soil nutrient distribution within a smallholder farm. In general, the major underlying drivers that affect the soil  $K_{ex}$  distribution in

these two typical smallholder farms in South India are vegetation, soil moisture, soil crust, and topographic attributes.

#### 4.2. Comparison of soil prediction models with different spatial resolutions

The Landsat 8-based soil models (Model KB1 and MB1) may filter out short-range variation of soil properties in smallholder farmland. Agriculture in Asia is characterized by smallholders cultivating small plots of land. According to the report from NCEUS (2008), about 81 percent of farms in India have land-holdings of less than 2 ha. It is possible that the coarse soil prediction maps, especially those based on Landsat 8 images, mixed the cultivated land from different farmers, soil types, and crop types. In such a case, Landsat 8-based soil prediction models probably have limited capability for the “Knowledge Brokers” and “Agricultural Extension Experts” to help smallholder farmers with soil nutrient management. However, the Landsat 8-based soil  $K_{ex}$  models such as KB1 and MB1 had relatively higher prediction accuracy compared with the RapidEye-based soil  $K_{ex}$  models in both study areas. The results from this research accord with some studies showing the prediction accuracy of relatively coarse spatial resolution soil prediction models can provide comparable or even higher prediction accuracy of soil properties compared with fine spatial resolution soil

prediction models (Shi et al., 2012; Steinberg et al., 2016). The disadvantages of coarse spatial resolution of Landsat 8 were compensated by its advantage of fine spectral resolution. In addition, many researchers have also indicated that fine spatial resolution datasets are required only in morphologically more complex areas (Cavazzi et al., 2013; Thompson et al., 2001). On contrast, Masuti and Kothapally village are both relatively flat homogenous areas. The use of detailed spectral indices is indispensable if edaphic conditions and landscape attributes were relatively homogeneous at coarse spatial resolutions. As a result, Landsat-based soil  $K_{ex}$  models still attained fair prediction accuracy in these two smallholder farms.

Because Landsat 8 image has a larger spectral range and more bands compared with the RapidEye image, and the WorldView-2 image has finer spatial resolution and more bands compared with the RapidEye image, the RapidEye image does not have evident strength in terms of its spatial and spectral resolutions compared with other images. RapidEye-based soil  $K_{ex}$  prediction models attained the lowest prediction fit and higher prediction error in both study areas. However, RapidEye-based soil prediction maps still showed strong capability to discern the soil nutrient variation in small farmland compared with Landsat 8-based soil prediction maps.

Very High Resolution (VHR) images-based soil prediction models have obvious advantages of characterizing soil spatial patterns at small agricultural fields, as fine spatial resolution images provides “detailed” and “unmixed” vegetation and ground surface information. In addition, WorldView-2/GeoEye-1/Pleiades-1A-based soil  $K_{ex}$  prediction models attain fair prediction accuracy. However, extensive use of VHR images-based soil prediction models in regional scales is neither practical nor economical due to the large data size, long image processing time, and high expense of image purchasing. The lack of SWIR and TIR bands in commercial VHR images and high spectral variation and shadows caused by canopy and topography may also affect the estimation of soil properties (Lu, 2006). The general short spectral range (visible and NIR region) in VHR images gives them a limited ability to characterize soil temperature, moisture, and biomass. In addition, the spatial pattern of soil properties in smallholder farm settings may also be affected by micro-scale topographic attributes and human agricultural practices. Those factors also can not be characterized by fine spatial resolution spectral indices. As a result, the VHR images-based soil  $K_{ex}$  models do not necessarily have higher prediction accuracy than Landsat 8-based soil  $K_{ex}$  models.

This research concluded that the utilization of remote sensing images with fine spatial resolution would not necessarily increase the prediction accuracy of soil  $K_{ex}$  prediction models in both study areas. The end users of DSM in smallholder farm settings need consider the spatial resolution, band width, spectral resolution, temporal frequency, cost, and processing time of different remote sensing sensors. In addition, the choice of spectral indices and the predicted soil property also need be considered. As a result, the selection of the appropriate remote sensing images in DSM is context-dependent because no “perfect” remote sensing product exists.

#### 4.3. Promotion of remote sensing-based DSM in soil nutrient management

Soil nutrients such as  $K_{ex}$ , available phosphorus ( $P_{av}$ ) and total nitrogen (TN) deficiency occur in smallholder farms in South India (Chander et al., 2014; Sadanandan et al., 2002). As a result, it is imperative to map the soil nutrient status and identify the farmland with soil nutrient deficiency in smallholder villages. The soil maps in this research can help smallholder farmers adopt appropriate soil

and water conservation practices. Different from some soil prediction models which utilized environmental variables such as soil depth, precipitation, temperature, geology, land use, soil historical data, soil class (Lamsal and Mishra, 2010; Vacca et al., 2014), each soil prediction model only utilized two remote sensing images. As a result, this research suggested soil prediction models utilizing only limited remote sensing images have potential to be promoted to the smallholder farm settings.

The research suggests WorldView-2/Pleiades-1A/GeoEye-1-based soil prediction models can provide more field-specific soil management suggestions to smallholder farmers. Those subtle characterizations of soil properties are important to assess the soil nutrient status for individual households. Landsat 8-based soil prediction models have fair prediction accuracy and do not need image purchase. They also have high potential to be widely applied in large scale. The empirical guidelines of remote sensing image selection and spectral indices selection have potential to be extended to other DSM research in fine scale agro-ecosystems such as smallholder farm settings all over the world.

## 5. Conclusions

Spectral indices including band reflectance values, band ratios between visible bands, CI, ARVI and BSI had relatively strong correlations with soil  $K_{ex}$  in smallholder farm settings. The research also suggested that WorldView-2/Pleiades-1A/GeoEye-1-based and RapidEye-based soil prediction models would not necessarily have higher prediction performance than coarse spatial resolution Landsat 8-based soil prediction models. Although WorldView-2/Pleiades-1A/GeoEye-1-based soil prediction model can provide detailed and unmixed spatial pattern of soil  $K_{ex}$  in fine scale farmland, the widespread use of Very High Resolution image such as WorldView-2 in regional scale is not practical and economical due to the large data size, long image processing time, and high expense of image purchasing. Although Landsat 8-based soil prediction models required no image purchasing and are easy to implement, those models may filter out short-range variation of soil properties and mix the farmland from different farmers, thus having limited capability to provide field-specific soil recommendation to the farmers. As a result, the selection of appropriate remote sensing images in DSM is context-dependent since a “perfect” remote sensing product does not yet exist. The empirical guidelines of remote sensing image and spectral indices selection can be extended to other DSM research in fine scale agro-ecosystems. The research demonstrated that the remote sensing-based soil prediction models have high potential to be promoted to the smallholder farm settings, and help the smallholder farmers develop sustainable and site-specific soil management scheme.

## Acknowledgement

Funding for this project was provided by the grant award No. 1201943 “Development of a Geospatial Soil-Crop Inference Engine for Smallholder Farmers” EAGER National Science Foundation. The soil analysis was performed in the soil laboratory at the International Crops Research Institute for the Semi-Arid Tropics (ICRISAT) in Patancheru/Hyderabad, Telangana State, India. We thank Christopher M. Clingensmith at University of Florida, and other ICRISAT staff members and villagers of Kothapally for support with field sampling. We also thank Yiming Xu's PhD committee members Dr. Thomas K. Frazer and Dr. Vimala D. Nair for their guidance and commitment. A matching assistantship for Yiming Xu was provided by School of Natural Resources and Environment, University of Florida, and China Scholarship Council.

## Appendix A. Supplementary data

Supplementary data related to this article can be found at <http://dx.doi.org/10.1016/j.jenvman.2017.06.017>.

## References

- Bellon-Maurel, V., Fernandez-Ahumada, E., Palagos, B., Roger, J.-M., McBratney, A., 2010. Critical review of chemometric indicators commonly used for assessing the quality of the prediction of soil attributes by NIR spectroscopy. *TrAC Trends Anal. Chem.* 29, 1073–1081. <http://dx.doi.org/10.1016/j.trac.2010.05.006>.
- Belnap, J., Lange, O.L., 2013. *Biological Soil Crusts: Structure, Function, and Management*. Springer Science & Business Media.
- Blasch, G., Spengler, D., Itzerott, S., Wessolek, G., 2015. Organic matter modeling at the landscape scale based on multitemporal soil pattern analysis using RapidEye data. *Remote Sens.* 7, 11125–11150. <http://dx.doi.org/10.3390/rs70911125>.
- Cavazzi, S., Corstanje, R., Mayr, T., Hannam, J., Fealy, R., 2013. Are fine resolution digital elevation models always the best choice in digital soil mapping? *Geoderma* 195–196, 111–121. <http://dx.doi.org/10.1016/j.geoderma.2012.11.020>.
- Chander, G., Wani, S.P., Sahrawat, K.L., Dixit, S., Venkateswarlu, B., Rajesh, C., Rao, P.N., Pardhasaradhi, G., 2014. Soil test-based nutrient balancing improved crop productivity and rural livelihoods: case study from rainfed semi-arid tropics in Andhra Pradesh, India. *Arch. Agron. Soil Sci.* 60, 1051–1066. <http://dx.doi.org/10.1080/03650340.2013.871706>.
- Cressie, N., 1993. *Statistics for Spatial Data (Revised Edition)*. Wiley, N. Y.
- De Benedetto, D., Castrignanò, A., Rinaldi, M., Ruggieri, S., Santoro, F., Figorito, B., Gualano, S., Diacono, M., Tamborrino, R., 2013. An approach for delineating homogeneous zones by using multi-sensor data. *Geoderma* 199, 117–127. <http://dx.doi.org/10.1016/j.geoderma.2012.08.028>.
- Diggle, P.J., Tawn, J.A., Moyeed, R.A., 1998. Model-based geostatistics. *J. R. Stat. Soc. Ser. C Appl. Stat.* 47, 299–350. <http://dx.doi.org/10.1111/1467-9876.00113>.
- Finley, A.O., Banerjee, S., Carlin, B.P., 2007. spBayes: an R package for univariate and multivariate hierarchical point-referenced spatial models. *J. Stat. Softw.* 19, 1–24.
- Horneck, D.A., Sullivan, D.M., Owen, J.S., Hart, J.M., 2011. *Soil Test Interpretation Guide*. Oregon State University, Extension Service, Corvallis, Or.
- Kim, J., Grunwald, S., Rivero, R.G., 2014. Soil phosphorus and nitrogen predictions across spatial escalating scales in an aquatic ecosystem using remote sensing images. *IEEE Trans. Geosci. Remote Sens.* 52, 6724–6737. <http://dx.doi.org/10.1109/TGRS.2014.2301443>.
- Lamsal, S., Mishra, U., 2010. Mapping soil textural fractions across a large watershed in north-east Florida. *J. Environ. Manage.* 91, 1686–1694. <http://dx.doi.org/10.1016/j.jenvman.2010.03.015>.
- Liu, S., Peng, Y., Du, W., Le, Y., Li, L., 2015. Remote estimation of leaf and canopy water content in winter wheat with different vertical distribution of water-related properties. *Remote Sens.* 7, 4626–4650. <http://dx.doi.org/10.3390/rs70404626>.
- Lu, D., 2006. The potential and challenge of remote sensing-based biomass estimation. *Int. J. Remote Sens.* 27, 1297–1328. <http://dx.doi.org/10.1080/01431160500486732>.
- Maynard, J.J., Johnson, M.G., 2014. Scale-dependency of LiDAR derived terrain attributes in quantitative soil-landscape modeling: effects of grid resolution vs. neighborhood extent. *Geoderma* 230–231, 29–40. <http://dx.doi.org/10.1016/j.geoderma.2014.03.021>.
- National Commission for Enterprises in the Unorganized Sector (2008). New Delhi: NCEUS.
- Pons-Fernández, X., Cuadrat-Prats, J., Vicente-Serrano, S., 2004. Mapping soil moisture in the central Ebro river valley (northeast Spain) with Landsat and NOAA satellite imagery: a comparison with meteorological data. *Int. J. Remote Sens.* 4325–4350.
- Qi, J., Chehbouni, A., Huete, A.R., Kerr, Y.H., Sorooshian, S., 1994. A modified soil adjusted vegetation index. *Remote Sens. Environ.* 48, 119–126. [http://dx.doi.org/10.1016/0034-4257\(94\)90134-1](http://dx.doi.org/10.1016/0034-4257(94)90134-1).
- Rosentreter, R., Rai, H., Upreti, D.K., 2014. Distribution ecology of soil crust lichens in India: a comparative assessment with global patterns. In: Rai, H., Upreti, D.K. (Eds.), *Terricolous Lichens in India*. Springer, New York, pp. 21–31.
- Sadanandan, A., Peter, K., Hamza, S., 2002. Role of potassium nutrition in improving yield and quality of spice crops in India. *Haryana Int. Potash Inst. Switz.* 445–454.
- Santin-Janin, H., Garel, M., Chapuis, J.-L., Pontier, D., 2009. Assessing the performance of NDVI as a proxy for plant biomass using non-linear models: a case study on the Kerguelen archipelago. *Polar Biol.* 32, 861–871. <http://dx.doi.org/10.1007/s00300-009-0586-5>.
- Shi, X., Girod, L., Long, R., DeKett, R., Philippe, J., Burke, T., 2012. A comparison of LiDAR-based DEMs and USGS-sourced DEMs in terrain analysis for knowledge-based digital soil mapping. *Geoderma* 170, 217–226. <http://dx.doi.org/10.1016/j.geoderma.2011.11.020>.
- Sreedevi, T.K., Shiferaw, B., Wani, S.P., 2004. Adarsha Watershed in Kothapally Understanding the Drivers of Higher Impact: Global Theme on Agroecosystems Report No. 10. URL. <http://oar.icrisat.org/3681/>.
- Steinberg, A., Chabrilat, S., Stevens, A., Segl, K., Foerster, S., 2016. Prediction of common surface soil properties based on vis-NIR airborne and simulated EnMAP imaging spectroscopy data: prediction accuracy and influence of spatial resolution. *Remote Sens.* 8, 613. <http://dx.doi.org/10.3390/rs8070613>.
- Taylor, J.A., Jacob, F., Galleguillos, M., Prévot, L., Guix, N., Lagacherie, P., 2013. The utility of remotely-sensed vegetative and terrain covariates at different spatial resolutions in modelling soil and water table depth (for digital soil mapping). *Geoderma* 193–194, 83–93. <http://dx.doi.org/10.1016/j.geoderma.2012.09.009>.
- Thenkabail, P.S., Smith, R.B., De Pauw, E., 2000. Hyperspectral vegetation indices and their relationships with agricultural crop characteristics. *Remote Sens. Environ.* 71, 158–182. [http://dx.doi.org/10.1016/S0034-4257\(99\)00067-X](http://dx.doi.org/10.1016/S0034-4257(99)00067-X).
- Thomas, G.W., 1982. Exchangeable Cations. *Methods of Soil Analysis. Part 2. Chemical and microbiological properties, second ed.*, pp. 159–166.
- Thompson, J.A., Bell, J.C., Butler, C.A., 2001. Digital elevation model resolution: effects on terrain attribute calculation and quantitative soil-landscape modeling. *Geoderma* 100, 67–89. [http://dx.doi.org/10.1016/S0016-7061\(00\)00081-1](http://dx.doi.org/10.1016/S0016-7061(00)00081-1).
- Vacca, A., Loddo, S., Melis, M.T., Funedda, A., Puddu, R., Verona, M., Fanni, S., Fantola, F., Madrau, S., Marrone, V.A., Serra, G., Tore, C., Manca, D., Pasci, S., Puddu, M.R., Schirru, P., 2014. A GIS based method for soil mapping in Sardinia, Italy: a geomatic approach. *J. Environ. Manage. Monit. Hum. Impacts Landscapes Environ. Change Sustain.* 138, 87–96. <http://dx.doi.org/10.1016/j.jenvman.2013.11.018>.
- Vasques, G.M., Grunwald, S., Myers, D.B., 2012. Influence of the spatial extent and resolution of input data on soil carbon models in Florida, USA. *J. Geophys. Res. Biogeosciences* 117. <http://dx.doi.org/10.1029/2012JG001982> n/a–n/a.
- Wani, S.P., Singh, H.P., Sreedevi, T.K., Pathak, P., Rego, T.J., Shiferaw, B., Iyer, S.R., 2003. Farmer-participatory integrated watershed management: adarsha watershed, Kothapally India - an innovative and upscalable approach. *J. SAT Agric. Res.* 2, 1–27.
- Williams, P., Norris, K., 1987. *Near-infrared Technology in the Agricultural and Food Industries*, 330 pp.
- Xiong, X., Grunwald, S., Myers, D.B., Kim, J., Harris, W.G., Bliznyuk, N., 2015. Assessing uncertainty in soil organic carbon modeling across a highly heterogeneous landscape. *Geoderma* 251–252, 105–116. <http://dx.doi.org/10.1016/j.geoderma.2015.03.028>.
- Xu, Y., Smith, S.E., Grunwald, S., Abd-Elrahman, A., Wani, S.P., 2017. Incorporation of satellite remote sensing pan-sharpened imagery into digital soil prediction and mapping models to characterize soil property variability in small agricultural fields. *ISPRS J. Photogramm. Remote Sens.* 123, 1–19. <http://dx.doi.org/10.1016/j.isprsjprs.2016.11.001>.